

# Precision Electroweak Data and the Mixed Radion-Higgs Sector of Warped Extra Dimensions

John F. Gunion<sup>a</sup>, Manuel Toharia<sup>a</sup>, James D. Wells<sup>a,b</sup>

<sup>(a)</sup> *Physics Department, University of California, Davis, CA 95616*

<sup>(b)</sup> *MCTP, Department of Physics, University of Michigan, Ann Arbor, MI 48109*

## Abstract

We derive the Lagrangian and Feynman rules up to bilinear scalar fields for the mixed Higgs-radion eigenstates interacting with Standard Model particles confined to a 3-brane in Randall-Sundrum warped geometry. We use the results to compute precision electroweak observables and compare theory predictions with experiment. We characterize the interesting regions of parameter space that simultaneously enable a very heavy Higgs mass and a very heavy radion mass, both masses being well above the putative Higgs boson mass limit in the Standard Model derived from the constraints of precision electroweak observables. For parameters consistent with the precision constraints the Higgs boson physical eigenstate is typically detectable, but its properties may be difficult to study at the Large Hadron Collider. In contrast, masses and couplings are allowed for the physical radion eigenstate that make it unobservable at the LHC. A Linear Collider will significantly improve our ability to study the Higgs eigenstate, and will typically allow detection of the radion eigenstate if it is within the machine's kinematical reach.

**Introduction:** Warping an extra-dimensional space to produce a natural hierarchy between the Planck scale and the weak scale, as introduced by Randall and Sundrum (RS) in Ref. [1], must not be in violation of all precision electroweak experiments that have been performed to date. A number of investigations of the constraints on the RS model from precision electroweak data have been performed. The corrections to precision electroweak observables can be described by the Peskin-Takeuchi parameters  $S$  and  $T$  and can come both from the Higgs-radion sector [2, 3, 4] and from the Kaluza Klein excitation sector [5]. The constraints from requiring perturbativity for vector boson scattering have also been considered [6]. In this paper, we seek to refine and expand upon precision electroweak constraints on the Higgs-radion sector focusing on those regions of parameter space for which the KK excitations are too massive to have significant  $S$  and  $T$  contributions.

In the simplest model, two branes are separated in a 5-dimensional AdS space of curvature  $k$ , where  $k$  should be a small fraction of  $M_{\text{Pl}-5}$  (where  $G_5$  and  $M_{\text{Pl}-5} = 1/[16\pi G_5]^{1/3}$  are the 5-dimensional gravitational constant and Planck mass, respectively) in order for the general approach to be reliable. In this RS approach, the two branes are separated by a distance  $y$ , and are stabilized to the value  $y = y_0$  with appropriate dynamics. The setup creates the needed hierarchy  $m_W \sim M_{\text{Pl}} e^{-ky_0}$ , as long as  $ky_0 \sim 36$ .

The metric of the five-dimensional space can be written as

$$ds^2 = \left[ e^{-2\sigma} \eta_{\mu\nu} + \hat{\kappa} \left\{ e^{-2\sigma} h_{\mu\nu}(x, y) - \eta_{\mu\nu} c(y) r(x) \right\} + \hat{\kappa}^2 \eta_{\mu\nu} e^{2\sigma} a(y) r^2(x) \right] dx^\mu dx^\nu + \left[ 1 + \hat{\kappa} 2e^{2\sigma} e(y) r(x) + \hat{\kappa}^2 e^{4\sigma} f(y) r^2(x) \right] dy^2 \quad (1)$$

where  $\hat{\kappa}^2 = 1/M_{\text{Pl}-5}^3$  and  $r(x)$  is the non-canonically normalized radion field.<sup>1</sup> In the unphysical case of no radion stabilization (i.e., no radion mass)  $\sigma(y) = ky$  (in the bulk),  $c(y) = e(y) = 1$ ,  $a(y) = 1/4$  (for no  $r\partial_\mu r\partial^\mu r$  trilinear self interactions in this limit) and  $f(y) = 2$ . We assume that the Standard Model particles all live on the “SM brane” at  $y = y_0$  and the Planck scale is reachable only at the “Planck brane” at  $y = 0$ , where the graviton wave function is peaked. The induced metric on the SM brane up to second-order in the radion is

$$g_{\mu\nu}^{\text{ind}}(x, y_0) = \eta_{\mu\nu} \left[ e^{-2ky_0} - \hat{\kappa} c_0 r(x) + e^{2ky_0} a_0 \hat{\kappa}^2 r^2(x) \right] \quad (2)$$

where  $a_0 = a(y_0)$  and  $c_0 = c(y_0)$  are unknown constants that depend on the stabilization dynamics.

We can then apply this induced metric to the brane Lagrangian, and derive interaction terms between SM states and the radion. The radion  $r(x)$  is proportional to an ordinary 4-dimensional scalar field that is likely to be the lightest state associated with the warped extra dimensions [8]. The canonically normalized 4-dimensional quantum fluctuation radion field  $\phi_0(x)$  is related to  $r(x)$  by

$$\frac{c_0}{2} \hat{\kappa} e^{2ky_0} r(x) = \left( \frac{1}{\Lambda_\phi} \right) \phi_0(x), \quad (3)$$

---

<sup>1</sup>In the notation of Ref. [7],  $\hat{\kappa} = \epsilon$  (which is not related to the  $\epsilon$  of 4-dimensional regularization appearing below),  $k = m_0$  and  $ky_0 = m_0 b_0/2$ . The field  $r(x)$  has dimensions of mass<sup>3/2</sup>.

where in the no-back-reaction limit of  $c(y) = 1$  we would have  $\Lambda_\phi = \sqrt{6}M_{\text{Pl}}e^{-ky_0}$ . In general,  $\Lambda_\phi$  is the vacuum expectation value of a 4-dimensional field whose perturbations are related to the radion. Intuitively,  $\Lambda_\phi$  can also be thought of as the Planck-warped scale on the SM brane and it should be numerically not dramatically above the weak scale if warped geometry is the origin of the weak scale.

The scale  $\Lambda_\phi$  is crucial in two regards. First,  $\Lambda_\phi^{-1}$  sets the strength of interactions of the canonically normalized  $\phi_0(x)$  with matter. Second, it determines the masses of the KK tower of graviton excitations. In particular, the mass of the first KK excitation is given by  $m_1 = x_1 \frac{k}{M_{\text{Pl}}} \frac{\Lambda_\phi}{\sqrt{6}}$ , where  $x_1 \sim 3.8$  is the first zero of the  $J_1(x)$  Bessel function. Reliability of calculations in the RS approach requires that the ratio of the bulk curvature  $k$  to  $M_{\text{Pl}-5}$  be small, implying  $\frac{k}{M_{\text{Pl}}} \lesssim 0.1$ . For  $\Lambda_\phi = 5 \text{ TeV}$ ,  $k/M_{\text{Pl}} = 0.1$  gives  $m_1 = 750 \text{ GeV}$ , *i.e.* large enough that KK excitations will not make significant direct contributions to  $S$  and  $T$ . In fact, our main focus will be on still larger values of  $\Lambda_\phi$ . For this region of parameter space, only the Higgs-radion sector and non-renormalizable operators coming from integrating out the KK states will be important for computing  $S$  and  $T$ .

After some computation, the interactions of  $\phi_0$  with the SM vector fields up to order  $\phi_0^2$  are

$$\mathcal{L}_{\text{int}}(\hat{\kappa}^1) = - \left( \frac{1}{\Lambda_\phi} \right) \phi_0(x) \left[ M_V^2 V^\alpha V_\alpha + \epsilon \left( \frac{F^{\alpha\beta} F_{\alpha\beta}}{4} - \frac{M_V^2}{2} V^\alpha V_\alpha \right) \right] \quad (4)$$

$$\mathcal{L}_{\text{int}}(\hat{\kappa}^2) = \frac{4}{\Lambda_\phi^2} \phi_0^2(x) \left[ \frac{\eta}{2} M_V^2 V^\alpha V_\alpha + \epsilon \left( \frac{(2\eta - 1)}{16} F^{\gamma\delta} F_{\gamma\delta} - \frac{(2\eta + 1)}{8} M_V^2 V^\alpha V_\alpha \right) \right] \quad (5)$$

where we have defined  $\eta = a_0/c_0^2 = \mathcal{O}(1)$ . Thus, we have exchanged the two free parameters  $a_0$  and  $c_0$  of Eq. (2) for the two free parameters  $\Lambda_\phi$  and  $\eta$ . The  $\epsilon$  in the above equations is a remnant of the dimensional regularization requirement of working in  $D = 4 - \epsilon$  dimensions. For example, the trace of the energy-momentum tensor of a massive vector field is

$$T^V{}^\mu{}_\mu = -M_V^2 V^\alpha V_\alpha + \epsilon \mathcal{L}_V. \quad (6)$$

As the radion interacts via the trace of the energy-momentum tensor at one loop, one finds the term  $\epsilon \mathcal{L}_V$  in the interaction Lagrangian. The second-order term, Eq. (5), requires care in its expansion derivation and is not simply related to the trace of the energy momentum tensor.

There may exist a Higgs-radion mixing [9] term  $\mathcal{L} = \xi \partial h_0 \partial \phi_0$  derived from the SM-brane operator

$$\mathcal{L} = \xi \int d^4x \sqrt{g_{\text{ind}}} R(g_{\text{ind}}) H^\dagger H. \quad (7)$$

Therefore, the complication of Higgs-radion mixing must be taken into account when computing the effects of the radion-Higgs sector on precision electroweak data.

The mass eigenstates  $h$  and  $\phi$  can be obtained from the “geometry eigenstates” ( $h_0$  and  $\phi_0$ ) by suitable redefinitions,<sup>2</sup>

$$h_0 = d h + c \phi \quad (8)$$

---

<sup>2</sup>The  $a$  and  $c$  below are not related to the  $a(y)$  and  $c(y)$  functions defined earlier. We also note that our conventions for  $a, b, c, d$  are those of Ref. [7]. These differ in the sign of  $a$  and  $b$  from Ref. [2]. For computing  $a, b, c, d$  we employ the exact inversion procedures of [7] rather than the approximate small- $\xi$  procedures of [9].

$$\phi_0 = a \phi + b h \quad (9)$$

with

$$a = -\frac{\cos \theta}{Z} \quad b = \frac{\sin \theta}{Z} \quad (10)$$

$$c = \left( \sin \theta + \frac{6\xi v}{Z\Lambda_\phi} \cos \theta \right) \quad d = \left( \cos \theta - \frac{6\xi v}{Z\Lambda_\phi} \sin \theta \right). \quad (11)$$

In the above,  $Z$  and  $\theta$  are defined by

$$Z^2 = 1 + 6\xi(1 - 6\xi)v^2/\Lambda_\phi^2, \quad (12)$$

$$\tan 2\theta = 12\gamma\xi Z \frac{m_{h_0}^2}{m_{\phi_0}^2 - m_{h_0}^2(Z^2 - 36\xi^2\gamma^2)}, \quad (13)$$

where  $v = 246 \text{ GeV}$  and  $m_{h_0}$  and  $m_{\phi_0}$  are the Higgs and radion masses, respectively, for  $\xi = 0$ .

**Precision Electroweak Framework:** The most important corrections to precision electroweak observables are from the self-energies of gauge vector bosons. In order to compute these, we have derived the necessary Feynman rules from the Lagrangian given by Eqs. (4) and (5), and have included the effects of Higgs-radion mixing. The resulting Feynman rules appear in Fig. 1. These are employed to compute the  $S$  and  $T$  parameters:

$$S = \frac{4c_W^2 s_W^2}{\alpha} \left[ \frac{\Pi_{ZZ}(M_Z)}{M_Z^2} - \frac{\Pi_{ZZ}(0)}{M_Z^2} \right] \quad (14)$$

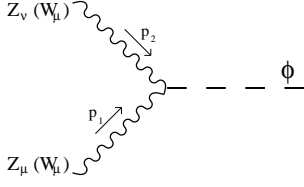
$$T = \frac{1}{\alpha} \left[ \frac{\Pi_{WW}(0)}{M_W^2} - \frac{\Pi_{ZZ}(0)}{M_Z^2} \right]. \quad (15)$$

For both  $S$  and  $T$  there are several types of contributions. Contributions of the first type,  $S_i$  and  $T_i$ , are from the sum over direct contributions of each eigenstate of the Higgs-radion system. Contributions of the second type,  $S^A$  and  $T^A$ , are the so-called anomalous terms from radion loop  $1/\epsilon$  poles being made finite by linear  $\epsilon$  terms in the expansion of the radion-matter interaction Lagrangian.

One also expects non-renormalizable operators to arise from integrating out the heavier states that are associated with the SM brane scale  $\Lambda_\phi$  and Kaluza-Klein excitations above that. They act as counter terms for divergences the radion creates from its non-renormalizable interactions with SM particles. Operators such as  $\mathcal{O} \sim (H^\dagger D_\mu H)^2$  break isospin symmetry and can have an important effect on the  $T$  parameter. Other operators can contribute to the  $S$  parameter. To account for these effects, we define the  $\mathcal{O}(1)$  parameters  $a_M$  and  $a_X$  equivalently to Eq. (12.5) of Ref. [2], and compute the non-renormalizable operator (NRO) contributions to  $S$  and  $T$ .

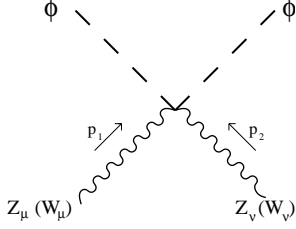
The values of each of the above contributions are given as follows:

$$S_i = -\frac{g_i^2}{\pi} \left( B_0(M_Z^2, m_i^2, M_Z^2) - \frac{B_{22}(M_Z^2, m_i^2, M_Z^2)}{M_Z^2} \right)$$



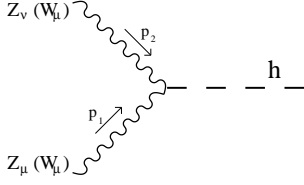
$$i g \frac{M_Z}{c_W} \eta_{\mu\nu} (c + a\gamma) - i\epsilon a V_{\mu\nu}^A$$

$$\left( i g M_W \eta_{\mu\nu} (c + a\gamma) - i\epsilon a V_{\mu\nu}^A \right) \quad (16)$$



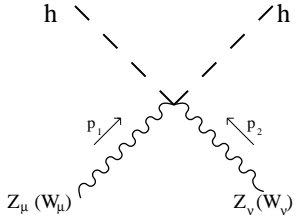
$$i \frac{g^2}{2c_W^2} \eta_{\mu\nu} (c^2 + 4a^2\gamma^2\eta) + i\epsilon a^2 W_{\mu\nu}^A$$

$$\left( i \frac{g^2}{2} \eta_{\mu\nu} (c^2 + 4a^2\gamma^2\eta) + i\epsilon a^2 W_{\mu\nu}^A \right) \quad (17)$$



$$i g \frac{M_Z}{c_W} \eta_{\mu\nu} (d + b\gamma) - i\epsilon b V_{\mu\nu}^A$$

$$\left( i g M_W \eta_{\mu\nu} (d + b\gamma) - i\epsilon b V_{\mu\nu}^A \right) \quad (18)$$



$$i \frac{g^2}{2c_W^2} \eta_{\mu\nu} (d^2 + 4b^2\gamma^2\eta) + i\epsilon b^2 W_{\mu\nu}^A$$

$$\left( i \frac{g^2}{2} \eta_{\mu\nu} (d^2 + 4b^2\gamma^2\eta) + i\epsilon b^2 W_{\mu\nu}^A \right) \quad (19)$$

$$V_{\mu\nu}^A = 2 \left( \frac{\gamma}{v} \right) \left[ \frac{1}{2} (p_1 \cdot p_2 \eta_{\mu\nu} - p_{1\mu} p_{2\nu}) + \frac{1}{2} M_V^2 \eta_{\mu\nu} \right] \quad (20)$$

$$W_{\mu\nu}^A = -2 \left( \frac{\gamma}{v} \right)^2 \left[ (2\eta - 1) (p_1 \cdot p_2 \eta_{\mu\nu} - p_{1\mu} p_{2\nu}) + (2\eta + 1) M_V^2 \eta_{\mu\nu} \right], \quad (21)$$

Figure 1: Feynman rules for vector couplings to the physical higgs and radion. In the figure,  $V_{\mu\nu}^A$  and  $W_{\mu\nu}^A$  are the anomalous contributions to the trilinear and quartic interactions,  $\gamma = \frac{v}{\Lambda_\phi}$  and  $c_W = \cos \theta_W$ , where  $\theta_W$  is the weak mixing angle. (Our  $\gamma$  differs by a factor of  $\sqrt{6}$  from the one defined in Ref. [2].)

$$-B_0(0, m_i^2, M_Z^2) + \frac{B_{22}(0, m_i^2, M_Z^2)}{M_Z^2} \Big) \quad (22)$$

$$S^A = \frac{v^2}{\pi \Lambda_\phi^2} \frac{1}{Z^2} \left( 5\xi - \frac{5}{6} - \left( \eta - \frac{1}{2} \right) \frac{M_\phi^2 \cos^2 \theta + M_h^2 \sin^2 \theta}{M_Z^2} \right) \quad (23)$$

$$S^{NRO} = \frac{v^2}{\pi \Lambda_\phi^2} \frac{1}{Z^2} \left( Z^2 a_X - \frac{(1 - 6\xi)^2}{12} \ln \frac{\Lambda_\phi^2}{M_Z^2} \right) \quad (24)$$

$$T_i = -\frac{g_i^2}{4\pi s_W^2} \left( B_0(0, m_i^2, M_W^2) - \frac{B_{22}(0, m_i^2, M_W^2)}{M_W^2} - \frac{B_0(0, m_i^2, M_Z^2)}{c_W^2} + \frac{B_{22}(0, m_i^2, M_Z^2)}{M_Z^2} \right) \quad (25)$$

$$T^A = \frac{6}{16\pi} \frac{v^2}{c_W^2 \Lambda_\phi^2} \frac{6\xi - 1}{Z^2} \quad (26)$$

$$T^{NRO} = \frac{3}{16\pi} \frac{v^2}{c_W^2 \Lambda_\phi^2} \left( -\frac{a_M}{3} + \frac{(1 - 6\xi)^2}{Z^2} \ln \frac{\Lambda_\phi^2}{M_Z^2} \right) \quad (27)$$

where the  $g_h$  and  $g_\phi$  are given by

$$g_h = d + b\gamma, \quad g_\phi = c + a\gamma, \quad (28)$$

and it is understood that we keep only the finite part in the Passarino-Veltman integrals [10].

The terms  $S_i$  and  $T_i$  give a positive (negative) contribution to  $S$  ( $T$ ), when increasing the scalar masses. The sign of  $T^A$  is positive (negative) for  $\xi > 1/6$  ( $\xi < 1/6$ ), and for  $\eta = 1/2$  the same statement applies for  $S^A$ . However, for  $\eta < 1/2$  ( $\eta > 1/2$ ),  $S^A$  is large and positive (negative) if  $m_\phi$  and/or  $m_h$  are large. Finally, the terms  $S^{NRO}$  and  $T^{NRO}$  give a contribution to  $S$  ( $T$ ) that depends on the unknown model-dependent input parameters  $a_X$  ( $a_M$ ),  $\xi$  and  $\Lambda_\phi$ . We will choose to define  $a_X$  and  $a_M$  as the values at scale  $\Lambda_\phi$ . Evolution to scale  $m_Z$  then leads to the indicated logarithmic corrections that give an increasingly negative (positive) contribution to  $S$  ( $T$ ) as  $|\xi|$  is increased and/or the scale  $\Lambda_\phi$  is lowered. In our numerical work, we assume  $a_M = a_X = 0$  at the scale  $\Lambda_\phi$  (i.e. we neglect the effects of the NRO at this scale). So long as  $a_M$  and  $a_X$  are  $\mathcal{O}(1)$ , the induced logarithmic terms are dominant in any case. Although these logarithmic NRO terms that appear in the running of the NRO's from  $\Lambda_\phi$  to  $M_Z$  can be present even when  $\xi = 0$ , they play a major role in the overall computation of  $S$  and  $T$  only when  $\xi \neq 0$  and the radion-Higgs mixing effect is large. In the end, we see that since the  $S$  and  $T$  contributions of the different types can have opposite (compensating) signs,  $S$  and  $T$  can be kept modest in size even when the radion and Higgs masses are large, provided  $\Lambda_\phi$  and  $\xi$  are appropriately chosen.

The main difference between this work and that of [2] at this analytical level is the presence of the  $(\eta - \frac{1}{2})$  term in Eq. (23). The value of  $\eta$  is model dependent and expected to be  $\mathcal{O}(1)$ . Because  $(\eta - \frac{1}{2})$  multiplies terms containing  $m_\phi^2$  and  $m_h^2$  in the  $S^A$  expression, the value of  $\eta$  is

of importance in determining the  $S, T$  constraints when either or both of these masses is large. Many of our results are presented for the  $\eta = 1/4$  value for which  $r(x)$  cubic self interactions of the form  $r\partial^\mu r\partial_\mu r$  are absent at order  $\hat{\kappa}^2$  in the Lagrangian resulting after the metric expansion. Physically, this implies absence of the related tadpole diagram for the radion.

**Higgs Boson and Radion Masses Consistent with Precision Constraints:** We now turn to numerical results for the precision electroweak predictions in the event that the Higgs boson and radion mix heavily through the operator of Eq. (7). Our purpose here is to build on the results of Refs. [2, 3, 4] by confronting our second-order Higgs-radion Lagrangian with a fully correlated  $S$  and  $T$  parameter fit to the precision electroweak data.

We primarily wish to show what parameter space looks like in the case that both mass eigenstates of the Higgs-radion system are above the SM Higgs boson 95% C.L. mass limit of 219 GeV as derived from precision electroweak data [11]. Such heavy Higgs mixed eigenstates have important implications for future collider physics programs [9, 7, 12, 13] and we wish to point out what is required of the theory in order that such heavy scalars not be inconsistent with existing constraints. We will also illustrate the precision data constraints at large  $|\xi|$  for cases where the Higgs eigenstate has a modest mass.

Given current limits on the radion mass and the mass scale  $\Lambda_\phi$ , where the Kaluza-Klein states should approximately reside, pure radion effects on precision electroweak data are small (although in the very large radion mass regime, the finite anomalous term  $S^A$  [Eq. (23)] might become important). The larger effects come when the radion mixes with the Higgs boson and the large couplings of the Higgs boson are shared among two states of differing masses. It is this effect we focus on by assuming that the radion-Higgs mixing coefficient has magnitude  $|\xi| \sim \mathcal{O}(1)$ .

In order to determine the allowed regions of  $S, T$  parameter space, we have employed a recent  $\chi^2$  ellipse parameterization [11]. The precise parameterization employed is

$$\Delta\chi^2 = \frac{(S - S^0)^2}{(0.11)^2} + \frac{(T - T^0)^2}{(0.09)^2} - 2 \frac{(S - S^0)(T - T^0)}{(0.11)(0.09)(0.735)(1 - [0.735]^2)} \quad (29)$$

where  $S^0 = 0.03$  and  $T^0 = 0.12$  are the preferred values of  $S$  and  $T$  relative to those computed in the SM for  $m_{H_{SM}} = 150$  GeV. For two parameters, the 68.27% ( $1\sigma$ ) and 90% Confidence Levels (CL) correspond to  $\Delta\chi^2 = 2.3$  and  $\Delta\chi^2 = 4.61$ , respectively.

We begin by considering the implications of the precision electroweak data for scenarios in which the physical eigenstate masses  $m_h$  and  $m_\phi$  are both very modest in size but  $|\xi|$  is large. To illustrate the impact, we consider  $\eta = 1/4$  and give some results for  $m_h = 120$  GeV in Fig. 2. (For this low a value of  $m_h$  and for the moderate values of  $m_\phi$  appearing in the plot, the term proportional to  $(\eta - 1/2)$  in Eq. (23) has very little impact and graphs for  $\eta = 1/2$ , for example, are indistinguishable from those for  $\eta = 1/4$ .) This figure shows that the large- $|\xi|$  wings of the theoretically allowed hourglass-shaped region in  $(\xi, m_\phi)$  parameter space are disfavored by the precision data. This result has important implications for collider searches. As shown in Ref. [13], for these same choices of  $\Lambda_\phi = 5$  TeV and  $m_h = 120$  GeV, the LHC is not guaranteed to find either the radion or the Higgs boson when  $\xi$  lies near the edges of the hourglass boundary (especially the  $m_\phi < m_h$ ,  $\xi > 0$  and  $m_\phi > m_h$ ,  $\xi < 0$  boundaries). In particular, near these boundaries, the  $gg \rightarrow h \rightarrow \gamma\gamma$  rate is suppressed. For  $m_\phi > m_h$ ,  $\xi < 0$  and  $m_\phi < m_h$ ,  $\xi > 0$  this

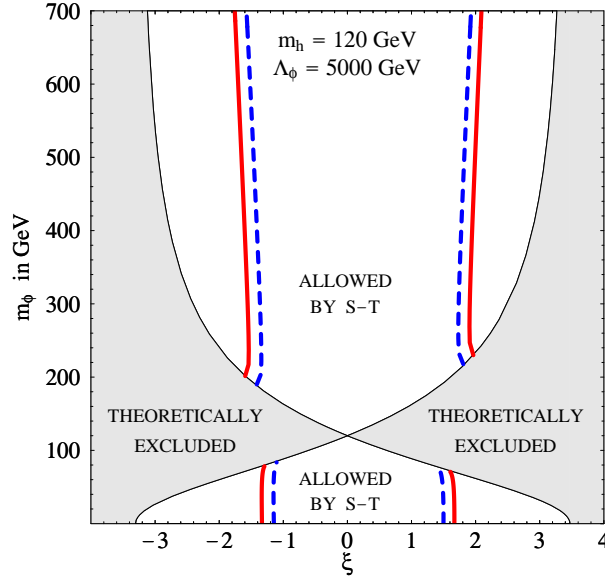


Figure 2: Allowed and disallowed regions in  $(\xi, m_\phi)$  parameter space, assuming  $\Lambda_\phi = 5$  TeV,  $m_h = 120$  GeV and  $\eta = 1/4$ . Regions within the theoretically allowed hourglass shape that are excluded at the 68% and 90% confidence level are those with  $|\xi|$  values larger than given by the thick dashed (blue) and solid (red) curves, respectively.

is largely because the  $ggh$  coupling is suppressed (due to the additional anomalous component). In addition, for  $m_\phi > m_h$  the  $WW_h$  coupling is suppressed in the vicinity of both the  $\xi > 0$  and  $\xi < 0$  boundary, implying suppression of the (dominant)  $W$ -loop contribution to the  $\gamma\gamma h$  coupling. The precision constraints are important in that they disfavor large  $|\xi|$  when  $m_h$  is modest in size. LHC discovery of the  $h$  will be possible throughout all of the  $(\xi, m_\phi)$  parameter space region allowed at 90% CL except for small (almost negligible for integrated luminosity of  $L = 300 \text{ fb}^{-1}$  at the LHC) regions along the  $m_\phi > m_h$ ,  $\xi < 0$  and  $m_\phi < m_h$ ,  $\xi > 0$  hourglass boundaries. Of course, even for parameter choices outside the 90% CL region that are such that the LHC is unable to see either the  $h$  or  $\phi$ , detection of the  $h$  would always be possible at a linear collider. In particular, the  $e^+e^- \rightarrow Zh$  mode yields a viable signal even for  $g_{ZZh}^2$  as low as 0.01, whereas  $g_{ZZh}^2 > 0.1$  throughout all of the theoretically allowed  $(\xi, m_\phi)$  parameter space plotted in Fig. 3. In contrast,  $g_{ZZ\phi}^2 < 0.01$  in much of the allowed  $(\xi, m_\phi)$  parameter space, implying that  $\phi$  detection would typically be very problematical.

We now turn to the regions of parameter space with  $m_h$  far above the 219 GeV SM Higgs mass limit. We will consider  $m_h = 350$  GeV and  $m_h = 650$  GeV and large negative values of  $\xi$ . (Results for large  $\xi > 0$  values are similar in nature.) In our first plot, Fig. 3, we fix the Higgs mass *eigenvalue* to  $m_h = 350$  GeV, and show 90% confidence level contours of allowed regions and disallowed regions in the  $m_\phi$ - $\Lambda_\phi$  plane. Of course, when  $\xi \neq 0$  it is mere convention to decide what is the “Higgs” state and what is the “radion” state, especially when they are close in mass. We follow the choice of [7] in which the Higgs boson is defined as the state that becomes the Standard Model Higgs in the limit  $\xi \rightarrow 0$ .



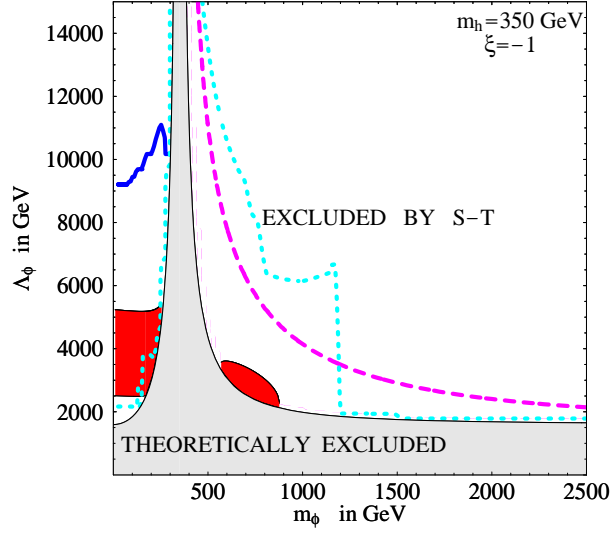


Figure 3: Precision electroweak allowed [solid (red) regions] and disallowed regions (at 90% CL) of the radion mass as a function of  $\Lambda_\phi$ , while holding fixed  $m_h = 350$  GeV and  $\xi = -1$ . The masses of the Higgs and radion physical eigenstates can be greater than the SM Higgs boson precision electroweak 95% CL upper limit of 219 GeV. The thick (pink) dashed line to the right of the theoretically disallowed tower is the LHC contour for  $r^h \equiv N_{SD}^h/N_{SD}^{SM} = 0.9$  – to the right of this contour  $0.9 < r^h < 1$ . The thick (blue) solid line to the left of the tower is the contour for  $r^h = 1.1$  – above this contour  $1 < r^h < 1.1$ . Between the tower and the thinner dotted (cyan) line,  $N_{SD}^\phi > 5$ . See text for more details.

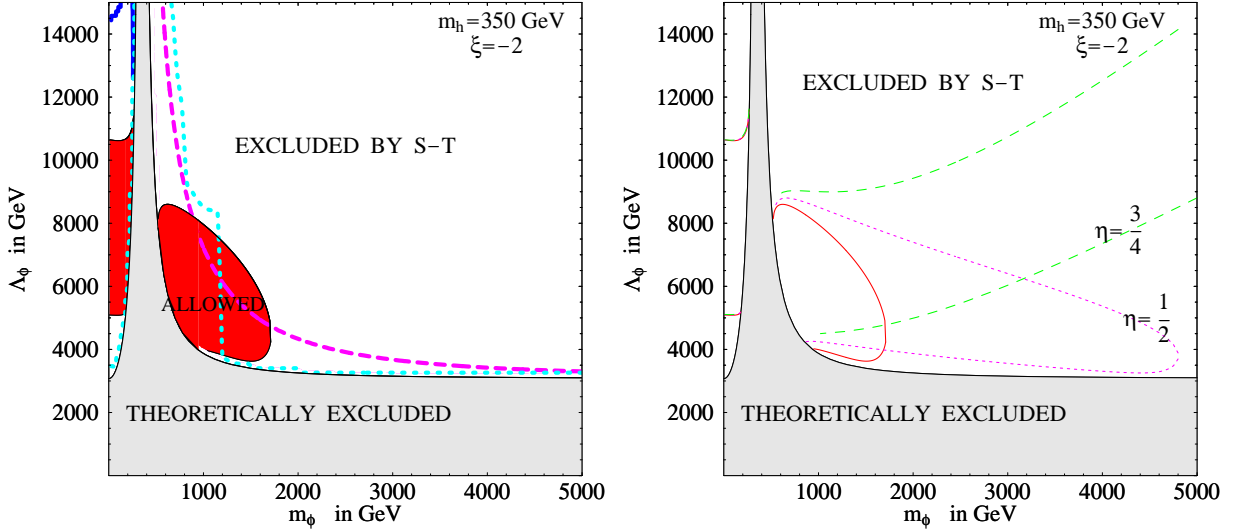


Figure 4: As in Fig. 3 but for  $\xi = -2$ . Results for  $\eta = 1/4$  are presented in the left-hand plot. This allowed region is compared to the regions allowed for  $\eta = 1/2$  and  $\eta = 3/4$  in the right-hand plot. In the latter, the region at low  $m_\phi$  is the same for all three  $\eta$  values. The LHC  $N_{SD}$  lines in the left-hand plot are as described for Fig. 3.

The lightly shaded tower in this figure is “theoretically excluded” because it is impossible for both mass eigenstates to exist for the particular set of input values. For example, no value of  $\Lambda_\phi$  will allow  $m_\phi$  to be 350 GeV in Fig. 3 since large mixing of eigenstates does not allow both states to have the same eigenvalues. Hence, the excluded tower is peaked at  $m_\phi = 350$  GeV.

The darker (red, for those who are viewing it in color) shaded region is allowed by precision electroweak data. There are two regions allowed. What characterizes these two regions is  $\Lambda_\phi$  near the theoretically allowed minimum value, and  $m_\phi$  somewhat near the Higgs mass. We see that an extraordinarily heavy radion mass compared to the Higgs mass is too disruptive to the  $S$ - $T$  fits.

If we increase the magnitude of  $\xi$  to  $-2$ , see Fig. 4, we find that the allowed region increases substantially for the same value of  $\eta = 1/4$ . This is the general trend commented on in Ref. [3] — larger negative  $\xi$  usually leads to a larger allowed region for heavy Higgs and radion. In Fig. 4, we also compare results for  $\eta = 1/2$  and  $\eta = 3/4$  to those for  $\eta = 1/4$ . For  $\eta = 1/2$  the extra terms in  $S^A$  proportional to  $m_\phi^2$  and  $m_h^2$  are absent. Consistency with the precision data is possible for much larger values of  $m_\phi$ . For  $\eta > 1/2$  and  $m_h \leq 500$  GeV the precision constraints can be satisfied for arbitrarily large  $m_\phi$ , as illustrated by the non-closing  $\eta = 3/4$  band in Fig. 4. One need only choose the value of  $\Lambda_\phi$  so that the term in  $S^A$  of Eq. (23) proportional to  $m_\phi^2/\Lambda_\phi^2$  has the appropriate negative value to compensate the  $\Delta S > 0$  contribution from the (somewhat SM-like)  $h$ , thereby bringing the net  $S, T$  prediction back into the precision electroweak ellipse. This is possible for  $m_h \lesssim 500$  GeV, *i.e.* such that the  $\Delta T < 0$  contribution from the  $h$  is not so negative that the total  $T$  lies below the  $S, T$ -plane precision electroweak ellipse.

The pattern and scope of parameters that are consistent with precision electroweak data are further clarified in Figs. 5 and 6. One sees quite clearly that if the Higgs mass is as high as even 650 GeV it is still possible to have a similarly heavy radion and satisfy the precision electroweak data constraints as long as the magnitudes of  $\xi$  and  $\Lambda_\phi$  are both increased substantially. We can understand this type of behavior as a limit where the unmixed radion state interacts weakly with SM matter (large  $\Lambda_\phi$ ), and the SM Higgs state loses some of its coupling strength by mixing with the radion (large  $\xi$ ). However, it is vital to the success of this scenario that the unmixed radion state not have zero coupling to the SM states (infinite  $\Lambda_\phi$ ) as this extra, appropriate amount of coupling strength is what makes it possible for both scalar states to be heavy while maintaining consistency with electroweak precision data. If  $\Lambda_\phi$  were infinite, the radion state would be sterile (equivalent to a non-interacting singlet Higgs state), and mixing a sterile boson with the Higgs boson cannot increase the upper bound of the lightest mass eigenstate over that of the SM bound [14]. Therefore, the figures provide example demonstrations that  $\Lambda_\phi \rightarrow \infty$  is never consistent with precision electroweak data when  $m_h > 219$  GeV.

The  $m_h = 650$  GeV figures, 5 and 6, also further clarify the dependence on  $\eta$ . For both  $\xi = -2$  and  $\xi = -4$ , much more of the  $(m_\phi, \Lambda_\phi)$  parameter space is allowed for  $\eta = 1/2$  and  $3/4$  than for  $\eta = 1/4$ . However, since this value of  $m_h$  is  $> 500$  GeV, for  $\eta = 3/4$  there is no allowed band of arbitrarily large correlated values of  $m_\phi$  and  $\Lambda_\phi$ . Still, as in the  $m_h = 350$  GeV case, the model-dependent terms in  $S^A$  are playing a major role — they prevent a firm conclusion regarding the exact portion of the large- $m_\phi, \Lambda_\phi$  part of parameter space that is excluded by the precision data.

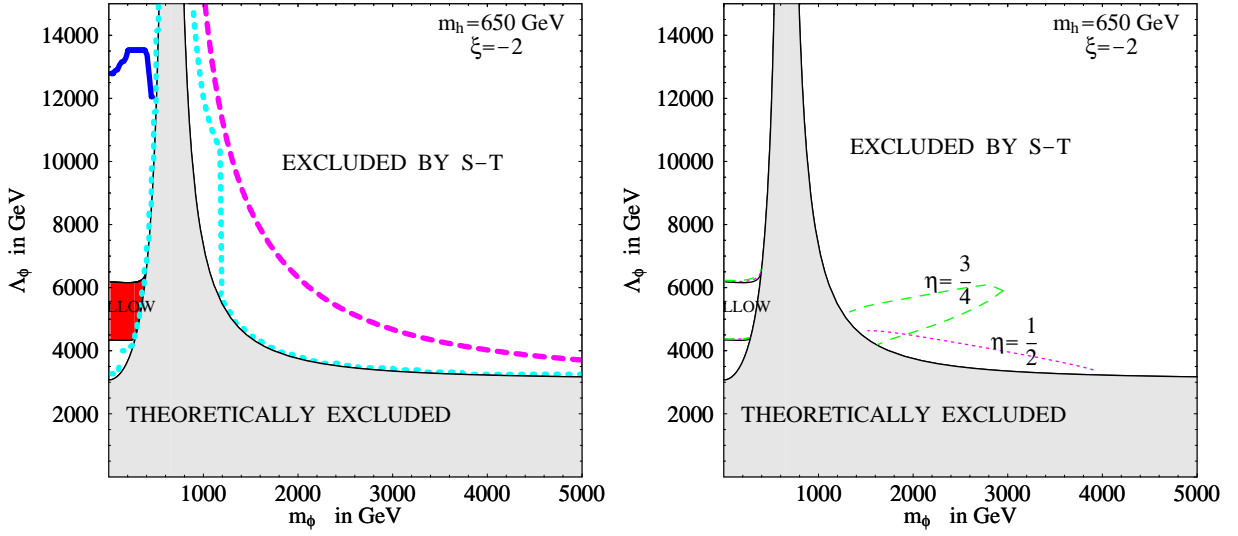


Figure 5: Allowed and disallowed regions (at 90% CL) of the radion mass as a function of  $\Lambda_\phi$ , while holding fixed  $m_h = 650$  GeV and  $\xi = -2$ . Results for  $\eta = 1/4$  are shown in left-hand plot. The LHC  $N_{SD}$  lines in the left-hand plot are as described for Fig. 3. The right-hand plot shows that large  $m_\phi$  is not excluded for  $\xi = -2$  when  $\eta = 1/2$  or  $3/4$ .

Comparing the figures of  $m_h = 350$  GeV with those of  $m_h = 650$  GeV, we see that the allowed region of lower radion mass appears to survive with increasing Higgs mass whereas the allowed region of heavier radion mass needs ever-increasing  $|\xi|$  to be viable when  $\eta \leq 1/2$ . We should keep in mind that these larger values of  $\xi$  might not be easy to generate in the more fundamental theory, as naive dimensional analysis suggests that  $|\xi|$  should not be more than  $\mathcal{O}(1)$ .

Nevertheless, the general conclusion stands that a heavy Higgs boson mass and a heavy radion can both be above the putative Higgs mass upper limit from precision electroweak data. Not only is this an example of a case where the Higgs boson limit can be evaded, but it is also an uncommon [15] example of a case for which it becomes *more difficult* to find correlating phenomena as the Higgs boson gets more massive. It is more difficult because  $\Lambda_\phi$  and  $m_\phi$  are also getting larger. This issue is especially clear if  $m_\phi > m_h > 500$  GeV with large  $|\xi| \gg 1$ . Although this scenario may not be as likely because  $\Lambda_\phi \gg m_W$  is necessary, it remains an interesting counterexample to the many models in which other phenomena emerge more and more strongly as  $m_h$  increases.

**Collider Detection:** Of course, a crucial question is whether the heavy Higgs and/or heavy radion eigenstates will be detectable at future colliders. To answer this question we followed the procedures of Refs. [16, 17]. In particular, we estimated the statistical significances for detection of the  $h$  or  $\phi$  ( $N_{SD}^i = S^i/\sqrt{B^i}$ ,  $i = 1, \dots, 8$ ) for the eight general Higgs boson detection modes so far rigorously studied at the LHC by the ATLAS and CMS groups [18]. These are (with  $\ell = e, \mu$ ): 1)  $gg \rightarrow h/\phi \rightarrow \gamma\gamma$ ; 2) associated  $Wh/\phi$  or  $t\bar{t}h/\phi$  production with  $\gamma\gamma\ell^\pm$  in the final state; 3) associated  $t\bar{t}h/\phi$  production with  $h/\phi \rightarrow b\bar{b}$ ; 4) associated  $b\bar{b}h/\phi$  production with

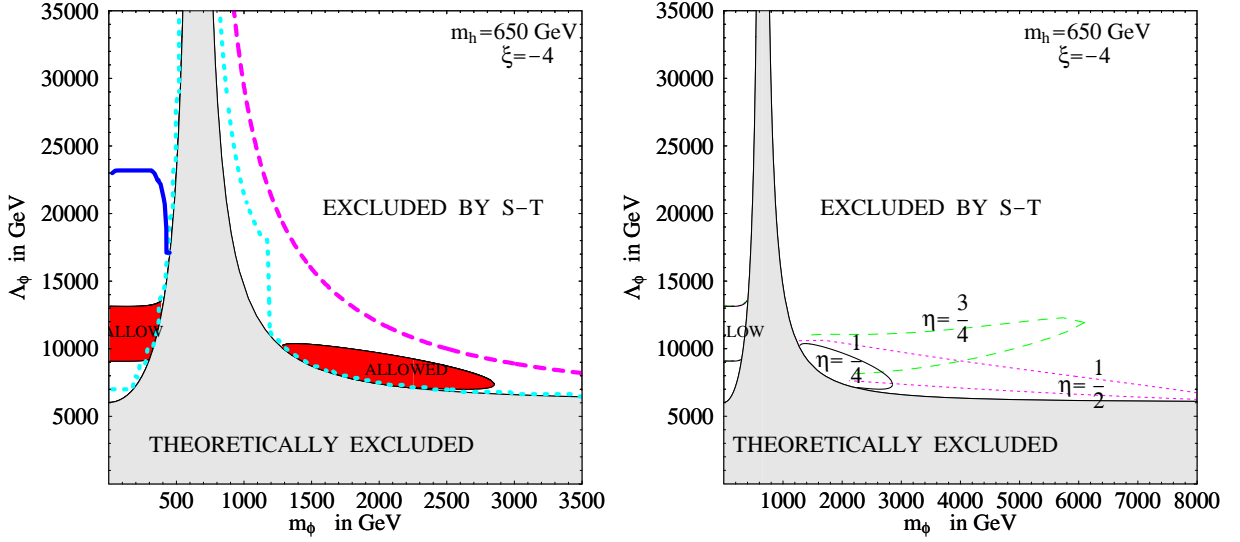


Figure 6: Allowed and disallowed regions (at 90% CL) of the radion mass as a function of  $\Lambda_\phi$ , while holding fixed  $m_h = 650$  GeV and  $\xi = -4$ . The left-hand plot shows that the heavy radion region is again allowed for  $\eta = 1/4$  because we have increased the magnitude of  $\xi$ . The LHC  $N_{SD}$  lines are as described for Fig. 3. In the right-hand plot (note the change of scale on the  $m_\phi$  axis), we show the variation of the allowed region with  $\eta$ .

$h/\phi \rightarrow \tau^+\tau^-$ ; 5)  $gg \rightarrow h/\phi \rightarrow ZZ^{(*)} \rightarrow 4\ell, 2\ell 2\nu$ ; 6)  $gg \rightarrow h/\phi \rightarrow WW^{(*)} \rightarrow \ell^+\ell^-\nu\bar{\nu}, \ell\nu jj$ ; 7)  $WW \rightarrow h/\phi \rightarrow \tau^+\tau^-$ ; 8)  $WW \rightarrow h/\phi \rightarrow WW^{(*)}$ . For each mode, we rescale the reference prediction for  $N_{SD}^i$  for a Higgs boson with the same mass as the  $h$  or  $\phi$  by using the  $h$  or  $\phi$  couplings relative to the reference couplings. We then compute a net statistical significance as  $N_{SD} = [\sum_{i=1}^8 (N_{SD}^i)^2]^{1/2}$ . For the large  $m_h$  values considered here, only the modes 5) and 6) are relevant for the  $h$ . In the case of the  $\phi$ , these are the relevant modes once  $m_\phi > 2M_W$ . For lower  $m_\phi$ , all the modes can contribute and can produce a visible net signal if  $\Lambda_\phi$  is not large.

We find that the  $h$  can be detected in the entire theoretically allowed regions of Figs. 3, 4, 5 and 6, the only exception being  $m_h = 350$  GeV,  $\xi = -1$  where there is a very tiny set of points for which  $N_{SD} < 5$ . These are located within the right-hand (red) “allowed” blob but very close to the boundary between this blob and the theoretically excluded “tower”. An interesting question then is the extent to which the  $h$  has production rate(s) that differ measurably from expectations for a SM Higgs boson of the same mass. In the above figures, contours where  $r^h \equiv N_{SD}^h/N_{SD}^{SM} = 0.9$  (1.1) are shown by thick dashed pink (thick solid blue) lines. The 0.9 contour appears to the right of the tower, and to the right of the 0.9 contour (*i.e.* for either higher  $\Lambda_\phi$  or higher  $m_\phi$ )  $0.9 < r^h < 1$ ; at the LHC, distinguishing between the  $h$  and a SM Higgs boson of the same mass would be difficult in this region. The 1.1 contour appears to the left of the tower, and above the contour (higher  $\Lambda_\phi$ )  $1.0 < r^h < 1.1$ ; as shown, the precision data disfavor this region — in the 90% CL favored region, distinguishing the  $h$  from a SM Higgs boson would be possible. Also shown in each of these graphs is a thinner dotted (cyan) line surrounding the tower on either side. Between this dotted line and the boundary of the tower,

$N_{SD}^\phi > 5$ ; detection of the  $\phi$  at the LHC would be possible. (The detection region terminates for  $m_\phi \gtrsim 1.2$  TeV simply because reliable LHC studies are not available above this mass.) Thus, the general result is that we are unlikely to observe the  $\phi$  in much of the precision-electroweak-allowed region (exactly how much depends on the value of  $\eta$ ). However, for (almost) all of the precision-allowed region, the  $h$  will be detectable at the LHC, but not necessarily distinguishable from a SM Higgs boson of the same mass. A future linear collider (with adequate  $\sqrt{s}$ ) would always be able to detect the  $h$ . A more detailed study is required to assess  $\phi$  discovery prospects for those values of  $m_\phi$  that are accessible at a given  $\sqrt{s}$  for the LC.

**Conclusions:** To summarize, we have found that, in the RS scenario of warped space-time, very heavy Higgs and radion mass eigenstates can be consistent with current precision electroweak data, even if the new-physics scales are such that the new phenomena of the model associated with the KK graviton excitations are difficult to detect. However, essentially all of the parameter space in question is such that the  $h$  eigenstate will be detectable at the LHC. The  $\phi$  will not generally be detectable, most notably in the large portion of precision-electroweak-allowed parameter space for which  $m_\phi$  is beyond the LHC reach. The  $h$  state will always be detectable at a  $\sqrt{s} \gtrsim m_h + 2M_Z$  linear collider. For regions of precision-electroweak-allowed parameter space with large  $m_\phi$ ,  $\phi$  detection at the LC would require very high  $\sqrt{s}$ . In short, the only signal for the RS scenario at both the LHC and the LC could be a single rather heavy scalar state with Higgs-like properties but couplings that might or might not be distinguishable from those of a heavy SM Higgs boson of the same mass. Giga- $Z$  operation at a future LC would help greatly to clarify the situation. For example, by pinning down the precise  $S, T$  values, Giga- $Z$  results would provide a strong constraint on the  $\xi$  and  $m_\phi$  parameters of the RS model even if only the  $h$  is detected. The phenomenology for (a) discovery of a sufficiently light  $\phi$  at the LC (when  $m_h$  is large) and (b) Giga- $Z$  operation will be pursued in a future work [19].

## Acknowledgments

JFG and MT would like to acknowledge valuable conversations with B. Grzadkowski and D. Dominici. JFG and MT are supported by the U.S. Department of Energy and the Davis Institute for High Energy Physics. JDW is supported in part by the U.S. Department of Energy and the Alfred P. Sloan Foundation.

## References

- [1] L. Randall and R. Sundrum, Phys. Rev. Lett. **83**, 3370 (1999) [hep-ph/9905221].
- [2] C. Csaki, M. L. Graesser and G. D. Kribs, Phys. Rev. D **63**, 065002 (2001) [hep-th/0008151].
- [3] G. D. Kribs, “Physics of the radion in the Randall-Sundrum scenario,” in *Proc. of the APS/DPF/DPB Summer Study on the Future of Particle Physics (Snowmass 2001)* ed. N. Graf, eConf **C010630**, P317 (2001) [hep-ph/0110242].

- [4] P. Das and U. Mahanta, Phys. Lett. B **528**, 253 (2002) [hep-ph/0107162].
- [5] H. Davoudiasl, J. L. Hewett and T. G. Rizzo, Phys. Rev. D **63**, 075004 (2001) [arXiv:hep-ph/0006041].
- [6] T. Han, G. D. Kribs and B. McElrath, Phys. Rev. D **64**, 076003 (2001) [arXiv:hep-ph/0104074].
- [7] D. Dominici, B. Grzadkowski, J. F. Gunion and M. Toharia, hep-ph/0206192.
- [8] W. D. Goldberger and M. B. Wise, Phys. Lett. B **475**, 275 (2000) [hep-ph/9911457].
- [9] G. F. Giudice, R. Rattazzi and J. D. Wells, Nucl. Phys. B **595**, 250 (2001) [hep-ph/0002178].
- [10] We use the same definitions of the Passarino-Veltman functions as given in D. M. Pierce, J. A. Bagger, K. T. Matchev and R. j. Zhang, Nucl. Phys. B **491**, 3 (1997) [hep-ph/9606211].
- [11] LEP Electroweak Working Group, “A Combination of Preliminary Electroweak Measurements and Constraints on the Standard Model,” LEPEWWG/2003-1, <http://lepewwg.web.cern.ch/LEPEWWG/>. The  $\chi^2$  ellipse parameterization employed for our numerical results is our best eye-ball fit to the  $S, T$  68% CL ellipse (for  $U = 0$  and 150 GeV Higgs mass) appearing at <http://lepewwg.web.cern.ch/LEPEWWG/plots/winter2003/w03-stu-contours.eps>. We thank J. Erler for providing a confirming parameterization.
- [12] J. L. Hewett and T. G. Rizzo, hep-ph/0202155; T. G. Rizzo, hep-ph/0207113 and hep-ph/0209076.
- [13] M. Battaglia, S. De Curtis, A. De Roeck, D. Dominici and J. F. Gunion, hep-ph/0304245; K. Cheung, C. S. Kim and J. h. Song, Phys. Rev. D **67**, 075017 (2003) [hep-ph/0301002]; M. Chaichian, A. Datta, K. Huitu and Z. h. Yu, Phys. Lett. B **524**, 161 (2002) [hep-ph/0110035].
- [14] J. D. Wells, “Extra dimensions and the universal suppression of Higgs boson observables at high energy colliders,” *Proceedings of SUSY 2002 (DESY, Hamburg)*, hep-ph/0205328.
- [15] M. E. Peskin and J. D. Wells, Phys. Rev. D **64**, 093003 (2001) [hep-ph/0101342].
- [16] U. Ellwanger, J. F. Gunion, C. Hugonie and S. Moretti, arXiv:hep-ph/0305109.
- [17] U. Ellwanger, J. F. Gunion and C. Hugonie, arXiv:hep-ph/0111179.
- [18] CMS Collaboration, “Expected Observability of Standard Model Higgs in CMS with 100 fb<sup>-1</sup>”, CMS NOTE 1997/057. ATLAS Collaboration, “Detector and Physics Performance Technical Design Report Vol. II (1999)”, CERN/LHCC/99-15 p. 675–811. D. Zeppenfeld, R. Kinnunen, A. Nikitenko and E. Richter-Was, Phys. Rev. D **62** (2000) 013009. D. Zeppenfeld, in *Proc. of the APS/DPF/DPB Summer Study on the Future of Particle Physics (Snowmass 2001)* ed. N. Graf, eConf **C010630**, P123 (2001).
- [19] Work in progress.